Journal of Design Against Fatigue
https://minerva-aset.com/JDAF
MINERVA ASET ISSN 2976-940X

The Effect of Composite Coating on Dynamic Behavior of Glass/Epoxy and Carbon/Epoxy Archimedes Wind Turbine Blade: Considering Fluid Solid Interaction

Nabi Mehri Khansari*, Amin Moghtader-ahar
Faculty of Mechanical Engineering, Sahand University of Technology, Tabriz, Iran

P A P E R I N F O

Paper history:
Received 14 December 2024
Received in revised form 28 March 2025
Accepted 7 April 2025

Keywords:
Archimedes Spiral Wind Turbines (ASWT), Fluid Solid Interaction (FSI) analysis, coating, composite materials.

A B S T R A C T

This study investigates the enhancement of dynamic behavior of traditional metallic blades in Archimedes Spiral Wind Turbines (ASWT) through the use of composite coatings, particularly carbon/epoxy and glass/epoxy. The study employs a combination of modal analysis and numerical fluid-structure interaction (FSI) analysis to assess the aero-elastic performance and structural stability of both coated and uncoated metal blades under diverse aerodynamic conditions. Modal analysis highlights the impact of composite coatings on the natural frequencies and mode shapes of the blades, ensuring safety and structural integrity by preventing resonance with operational frequencies. Further FSI analysis shows that composite coatings significantly improve fatigue strength and increase the fatigue life of the metal blades by reducing stress concentrations and optimizing load distribution during operation. These findings emphasize the potential of composite-coated metal blades as a promising advancement in wind turbine technology, addressing both dynamic stability and long-term durability. Also, it is evident that coating the turbine blade with a composite material result in a notable increase in the maximum stress experienced by the blade. Specifically, this modification leads to a 15.7% rise in maximum stress. This increase is significant and suggests that the composite coating may alter the structural behavior of the turbine blade under operational conditions.

https://doi.org/10.62676/jdaf.2025.3.1.10

1. INTRODUCTION

Small-scale wind power generation equipment (100 kW or less) is typically used to power homes, farmland, or small commercial centers. In some remote locations that have to use diesel generators, the owners prefer to use wind turbines to avoid the need to burn fuels. In some cases, these turbines are used to reduce electricity purchase costs or to use clean electricity. Wind turbines connected to batteries are used to power remote homes. This study aims to design fabrication and analyze small-sized urban wind turbine blades as the most important part of the turbine. To enhance the portability of the turbine and facilitate its installation across diverse urban environments, the incorporation of lightweight composite and polymer materials in the structural design is being actively pursued. This approach aims to mitigate the overall weight of the turbine while maintaining structural integrity and performance. In this research, the 0.5 kW spiral turbine is considered. This type of turbine has a higher efficiency due to its structure, which can be improved by replacing the metal blade with a composite and precise design based on the interaction between the structure and the fluid. The general schematic of the frame and the base is as

*Corresponding Author: n.mehri@sut.ac.ir

Cite this article as: Nabi Mehri Khansari, Amin Moghtader-ahar, The Effect of Composite Coating on Dynamic Behavior of Glass/Epoxy and Carbon/Epoxy Archimedes Wind Turbine Blade: Considering Fluid Solid Interaction, ***Journal of Design Against Fatigue,*** Vol. 3, No. 1, (2025), 1-18, https://doi.org/10.62676/jdaf.2025.3.1.10

follows, which can be assembled in the opposite direction of the blades.

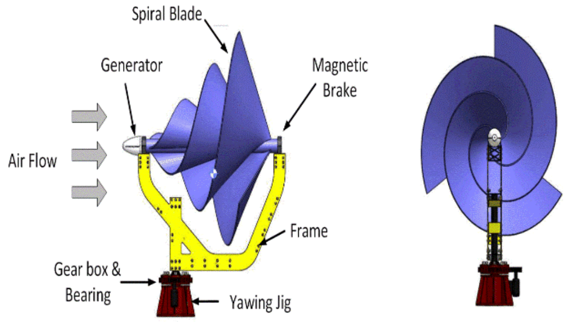

Figure 1 Schematic view of the studied turbine

Also, the blades of this type of turbine consist of at least three assembled blades, whose general profile will be as follows.

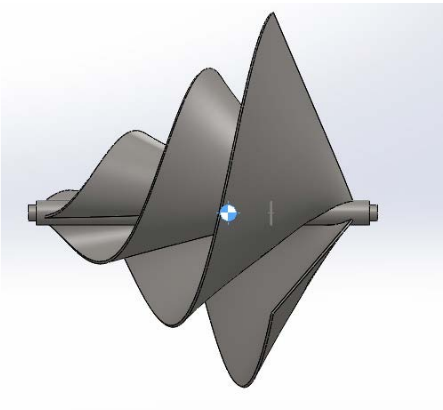

Figure 2 Side view of spiral turbine blade

All three blades are connected with an offset of 120 degrees around the axis of rotation, and each blade has a symmetrical arrangement concerning the turbine axis, which can be compared to a three-dimensional pyramid. The turbine blades can be used individually (instead of three blades) and can be designed and manufactured according to the different constraints resulting from the different working conditions. As for the type of blades, as mentioned above, they can be made of different materials, including metal, polymer, and metal-based composites. For example, for mountainous areas with a high probability of strong winds and hail throughout the year, it is better to use composite or composite with a metal liner to be a good shock absorber for different weather conditions. In the same way, for different climatic regions, there is the possibility of redesigning and structural changes, both in terms of geometry and material, and performance. In general, there are different types of wind turbines [1-4], which can be divided into two types: horizontal-axis wind turbines and vertical-axis wind turbines [5]. Horizontal axis wind turbines mostly consist of a propeller-type multi-bladed windmill in which the main rotor shaft is parallel to the wind direction. The vertical axis wind turbines are classified into two types, Savonius and Darrieus, and the rotor shaft is perpendicular to the wind, unlike the horizontal axis [3]. In most studies, the effects of blade geometry on the power curve, rated power of the turbine, and generated electricity have been investigated [6]. In this regard, Arens and Williams conducted a numerical study on the Darrieus vertical axis turbine, in which the airflow field on the roof of buildings with different shapes and certain geometric ratios was investigated [7]. In the mentioned study, the feasibility of installing vertical axis turbines on the roofs of houses was investigated [8, 9]. Scheurich and Brown [10] concluded in the numerical investigation of Darrieus turbines with a vertical axis that this type of turbine exhibits an inherent instability in the aerodynamic load under unstable flow conditions due to the continuous change in the angle of attack at the blades, which is less observable in examples with a horizontal axis. Archimedes spiral wind turbines, a new concept of horizontal axis turbines, are designed using Archimedes spiral principles. Unlike traditional vertical axis turbines that only use lift force to obtain power from wind energy, Archimedes spiral wind turbines use both lift force and drag force to absorb wind energy. This particular structure determines the special aerodynamic characteristics of small-scale wind turbines. The advantages of using an Archimedes spiral structure will be more obvious in many situations, such as around buildings because these wind turbines also operate at low wind speeds. Other advantages of this type of turbine include low noise due to relatively low rotation speed [11], although the disadvantage of the Archimedes wind turbine is the high thrust force compared to a conventional type of horizontal axis turbine blade, which makes a stronger structure for keep the turbine blades needed. In 2009, Timmer and Toet [12] conducted basic research to investigate the potential and optimal power output of the small spiral Archimedes wind turbine. The highest efficiency measured in their study was 12% [12]. Lu et al. [13] recently developed the Archimedes spiral wind turbine blade design method and reached numerical simulation using ANSYS CFX v12.1. From the aerodynamic point of view, it is possible to investigate the effects of diffusers in increasing the efficiency of wind turbines [14], predicting the performance coefficient by considering the three-dimensional dynamic behavior beyond the tip of the formed vortex [1], the effect of the intensity of environmental turbulence on small scale wind turbine performance [15] pointed out. The global market of small wind turbine systems is increasing at an approximate rate of 40 to 50% per year, however, small wind systems are not economically feasible due to their low efficiency, despite their great necessity and appropriate marketability [5, 11, 16]. Therefore, to increase the efficiency of small-size wind turbines, an innovative design is required. To solve this problem, Archimedes spiral blade wind turbine using Archimedes spiral principle has been recommended as a suitable solution [17]. Archimedes wind turbines usually produce electrical energy at wind working speeds of less than 3 meters per second [11]. Archimedes spiral blade had high power factor values in a wider range of tip speed ratios tested [6, 18]. In addition, this type of turbine has a prominent geometric feature that can increase the aerodynamic performance and maximize the lift and drag values [6, 17-20] In addition, in some references, the experimental and numerical study of aerodynamics and the characteristics of the Archimedes spiral wind turbine blade have been studied [12]. Recently, the market size of industrial wind power generators has grown exponentially due to their low-cost power generation and environment-friendly features. It is well established that, wind power is abundant and clean, and produces no greenhouse gas emissions during operation.

Wind power generation systems are generally classified by the size of wind turbines and electrical power capacity as large or small wind turbine systems [21]. The performance evaluation of small wind turbines under Variable Winds in Cities: A Case study applied to an Ayanz Wind turbines with screw blades showed significant improvements in performance and efficiency[22]. Analysis of Screw Turbine Design with additional flaps modification was done using computational fluid dynamics method[23, 24]. The small-sized system that produces electric power of less than 100 kW has been widely installed in urban and local areas for various purposes [3, 13, 25]. In addition, they are classified as horizontal axis wind turbines (HAWT) and vertical axis wind turbines (VAWT) according to the direction of the rotating shaft. In this research, the axis of the shaft is horizontal and therefore the current turbines are horizontal-axis wind turbines (HAWT). HAWTs consist of a propeller-type multi-bladed windmill and a tail vane (tail wing), where the main rotor shaft is parallel to the wind direction. VAWTs are of Savonius and Darrieus types, where the rotor axis is perpendicular to the wind. So far, several works have been reported to improve the efficiency of small wind turbines. Matsushima and his colleagues show the effect of the diffuser on increasing the efficiency of the wind turbine [14]. Howell et al. predicted the coefficient of performance by considering the three-dimensional dynamic behavior of the blade tip vortex [1]. Lubitz showed the effect of environmental turbulence intensity on the performance of a small-scale wind turbine [15]. Also, Kot et al. investigated the maximum power point tracking algorithms assigned to small wind turbines [26].

One of the critical aspects of the ASWT's design is its potential for improved fatigue life and strength, which are essential for the longevity and reliability of wind turbine blades. Fatigue failure in turbine blades can occur due to cyclic loading from wind forces, leading to structural degradation over time. The ASWT's spiral blades are designed to minimize stress concentrations and enhance load distribution, which can significantly improve their fatigue performance compared to traditional straight-blade designs [27]. Research indicates that optimizing blade angles and materials can further enhance the aerodynamic efficiency and fatigue resistance of these turbines [28]. Recent studies have employed computational fluid dynamics (CFD) simulations to analyze the aerodynamic characteristics of ASWT blades under various operating conditions. These simulations help identify optimal design parameters that enhance both performance and durability. For example, variations in blade angle were shown to influence aerodynamic performance significantly and affect fatigue life [29, 30]. Experimental validations of CFD results have demonstrated that the ASWT can maintain operational efficiency even at low wind speeds, which is crucial for urban applications where wind conditions are often less than ideal [31]. Integrating composite materials as coatings on metal blades has emerged as a promising approach to enhance fatigue strength and life. Composite coatings can provide improved resistance to environmental factors and mechanical stresses, thereby extending the operational lifespan of the blades [32]. This study examines the dynamic behavior of composite and metallic structures subjected to fluid flow loading, specifically wind forces. The primary objective is to analyze structural strength under dynamic load conditions caused by blade rotation and wind impact on the blade surface. The research focuses on identifying regions within the structure that exhibit lower strength compared to other areas and experimentally reinforcing these weak points. Given the fluctuating nature of aerodynamic loading and the structure's varying response to fluid dynamic forces, the investigation first identifies zones with maximum displacement and stress. Subsequently, coatings are applied to enhance both dynamic and static strength in these critical areas.

2. INVESTIGATING THE DYNAMIC BEHAVIOR OF SPIRAL WIND TURBINE (ASWT)

This study investigates the dynamic behavior of composite Archimedean spiral turbine (ASWT) blades under operational conditions, specifically analyzing carbon/epoxy and glass/epoxy materials through fluid-structure interaction (FSI) simulations. Using ANSYS software, fluid-induced forces, aerodynamic characteristics (e.g., pressure coefficient), and dynamic responses were evaluated numerically. While composite blades have not yet been employed to enhance turbine efficiency, this research highlights the necessity of detailed structural analysis and material optimization for performance improvement. The findings emphasize the relationship between blade material properties and hydrodynamic performance, providing insights for future design enhancements in spiral turbine applications.

Turbine design based on power and aerodynamic parameters

Based on Appendix A and Figure 1, the three blades are interconnected at an angle of 120 degrees, forming a structure comparable to a three-dimensional pyramid. The outer diameter of the 0.5 kW turbine measures 0.5 meters. The aerodynamic equations are derived under the following four assumptions:

1. The flow is considered incompressible and stable.
2. The fluid is treated as a control volume along the axis of rotation.
3. The mass flow rate remains consistent at the outlet boundary conditions for all three blades.
4. The relative speed at the outlet boundary conditions is assumed constant, with its direction tangential to the blade edge.

To calculate the torque and power of a small turbine with spiral blades, the momentum relationship for a control volume can be used:

$$\frac{\partial}{\partial t}\int_{CV}(r\times V)\rho dV+\int_{CS}(r\times V)\rho V.\hat{n}dA=\sum(r\times F) \tag{1}$$

The above relation represents the angular momentum based on the control volume. Under steady-state conditions, the first integral on the left side of Equation (5) becomes zero because it is independent of time. Consequently, the equation simplifies to the following:

$$\int_{CS}(r\times V)\rho V.\hat{n}dA=\sum(r\times F) \tag{2}$$

On the other hand, the continuity equation is expressed as follows, assuming constant conditions for the control volume:

$$\frac{\partial}{\partial t}\int_{CV}\rho dV+\int_{CV}\rho W.\widehat{n}dA=0 \tag{3}$$

Under steady-state conditions and assuming constant density in Equation (3), the first integral on the left side of the equation becomes zero. The second, non-zero part of the equation represents the total mass flow passing through the control volume. Consequently, Equation (3) can be rewritten as follows:

$$-\dot{m}_{in}+\dot{m}_{out}=0 \tag{4}$$

In the above relationship, the values can be determined based on the turbine's shape and dimensional parameters.

$$\dot{m}_{in}=\rho U_{\infty}\sin\gamma\times\pi\left(\frac{R_1+R_2}{2}\right)S_1 \qquad \dot{m}_{out}=3\rho A_{out}W_{\theta} \tag{5}$$

Where:

$$\gamma=\tan^{-1}\left(\frac{R_1}{S_1}\right) \tag{6}$$

The angle γ is defined as the angle between the rotation axis and the blade tip. Additionally, the following geometric parameters are specified:

- R_1: The vertical distance from the tip of the outer blade to the axis of rotation.
- R_2: The vertical distance from the tip of the inner blade to the axis of rotation.
- S_1: The horizontal distance between the tip of the front blade and the root of the spiral blade.

These parameters are summarized in Table 1.

Table 1: Effective parameters in blade design

Parameter	Definition of parameters
$\gamma=\tan^{-1}\left(\frac{R_1}{S_1}\right)$	The angle between the rotor axis and the tip of the blade
$\dot{m}_{in}$	The input mass flow rate to the control volume
$\dot{m}_{out}$	The output mass flow rate to the control volume
U_{∞}	Free flow speed
W_{θ}	Tangential component for relative velocity
V_{θ}	Tangential component for absolute velocity
W	Relative Velocity
α	The angle between V and V_{θ}
β	The angle between W and W_{θ}
K	turbulent kinetic energy
ω	Angular Velocity
R_1	The distance of the outer part of the blade, which is far from the hub or the center of rotation
R_2	The distance of the part of the blade that is closer to the hub or the center of rotation
$L_1(S_1)$	x is the distance between the center of the rear side and the position x, which is perpendicular to the tip of the outer blade
$L_2(S_2)$	The distance between the center position of the rear side and the x position and perpendicular to the tip of the inner blade
A_{out}	Estimated area of mass flow exit area

Also, the shape parameters and dimensions of 0.5 kW spiral turbine are shown in the Figure 3

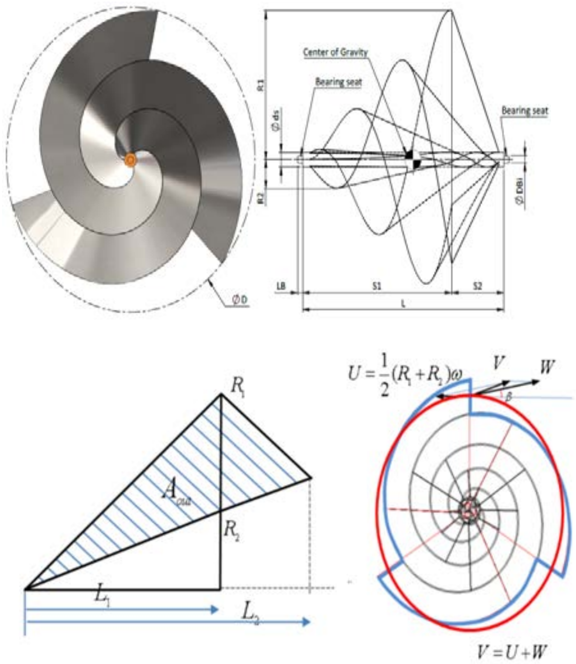

Figure 3 Shape parameters and dimensions of 0.5 kW spiral turbine under investigation

Relative velocity (W) refers to the speed at which the fluid (usually a gas or liquid) flows on the surface of the turbine blade relative to the blade itself. Takes into account mathematically, the relative velocity (W) can be expressed as the vector sum of the absolute velocity of the fluid (V) and the tangential velocity of the blade at a specific point on its surface: W = V + U. The relative velocity is essential to calculate the aerodynamic forces acting on the turbine blade and subsequently the energy conversion efficiency of the turbine.

Tangential velocity (U) specifically refers to the velocity of a point on the blade surface of an Archimedean spiral turbine in the direction tangential to the rotation of the blade. It represents the speed at which a point on the blade surface moves in a circle around the axis of rotation of the turbine. The tangential speed (U) can be calculated with this formula (U = R × ω) where U is the tangential velocity, R is the distance from the turbine rotation axis to the point on the blade surface and ω is the angular velocity that indicates the speed of rotation of the turbine blade in radians per unit of time. The tangential velocity is essential to understanding the rotational motion of the blade and its interaction with the fluid flow, as it contributes to the relative velocity mentioned above. Briefly, relative velocity is the combined velocity of fluid flow and tangential motion of the blade at a point on the turbine blade surface, while tangential velocity specifically refers to the velocity of that point on the blade in the tangential direction due to its rotation. These concepts are useful in the analysis and design of Archimedean spiral turbine blades for efficient energy conversion.

Absolute velocity (V) refers to fluid velocity regardless of turbine blade speed. It represents the velocity of the fluid measured at a point in space without considering the influence of the turbine. Absolute speed can be quantified using speed-measuring instruments such as anemometer or flow meter. It is significant in turbine design and operation because it provides information about the inlet flow conditions and helps determine the turbine's ability to extract energy from the fluid. In short, the relative velocity combines the fluid velocity and the tangential velocity of the turbine blade at a given point, while the tangential velocity refers specifically to the velocity of the blade in its direction of rotation. The absolute velocity is the fluid velocity regardless of the presence of a turbine. Figure 4 shows the triangle of speed U, V, W, and α is the middle angle between V and V_θ V_θ. It means the perpendicular component to the outlet boundary, and the absolute speed of V can be the following equation.

$$V^2 = W^2 + U^2 - 2WU\cos\beta$$
$$V_\theta = V\cos\alpha \tag{7}$$

$$\alpha = \sin^{-1}\left(\frac{W}{V}\sin\beta\right) \tag{8}$$

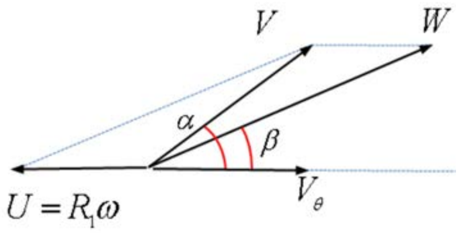

Figure 4: U, V and W velocity triangle

Wind speed data collected over an extended period, typically through measurements or historical records, can be analyzed using statistical methods to determine the parameters of the Weibull distribution that best fit the observed data. Once the distribution is fitted, it can be utilized for wind energy evaluation and planning various applications. The Weibull distribution is widely used in wind energy studies to model wind speed variations at specific locations over defined time periods. Its flexibility as a statistical distribution makes it particularly effective in describing the variability of wind speed.

$$f(x;\lambda,k) = \frac{k}{\lambda}\left(\frac{x}{\lambda}\right)^{k-1} e^{-(x/\lambda)^k} \tag{9}$$

In the above relation, X is the wind speed, λ scale parameter, and K is the shape parameter. K affects the shape of the distribution curve. Different locations may have diverse characteristics of wind speed and distribution, so fitting the Weibull distribution to the observed wind speed data helps to identify the wind source at a particular location. In this research, the written code uses the Weibull function to estimate the Weibull parameters from the whole year's wind speed data and then generates the Weibull distribution using the Weibull function. According to the research done for the Azerbaijan region, the wind speed distribution according to the probability distribution is shown in Figure 5.

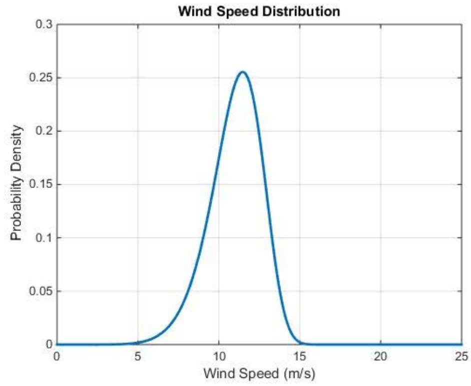

Figure 5 Probability distribution of wind speed for Azerbaijan region according to Weibull function

Power factor in terms of tip speed ratio (TSR)

The speed at which the outermost point of the turbine blade is moving is called the blade tip speed. The tip speed ratio (TSR) is a critical parameter in the design and performance of wind turbines and some hydro turbines. It defined the ratio of the tangential speed of the blade tip to the free flow speed of the fluid (air or water) in which the turbine operates. In the case of Archimedean spiral turbine blades, TSR evaluates like other types of turbines. The following formula calculates the tip speed ratio (TSR) for Archimedean spiral turbine blades.

$$TSR = \frac{R\omega}{V_\infty} \tag{10}$$

where ω , V_∞ , and R are the rotational speed of the blade, the speed of the fluid flow, and the radius of the rotor, which are determined specifically for each type of turbine. Also, the power factor of the rotor (Cp), which is the aerodynamic efficiency, can be defined as the ratio of the mechanical power output from the rotor to the input aerodynamic power. Now, using the mentioned relationships, the blade torque is obtained in the following way:

$$T_{shaft} = 3\rho V_\theta^2 \times \frac{(R_2 - R_1)}{6L_1(L_2 - L_1)} \times \left[R_2\left(2L_2^3 + L_1^3 + L_1L_2^3\right) - L_1R_1\left(L_1 + L_2\right)^2\right]$$
$$V_\theta = V\cos\alpha \tag{11}$$
$$\alpha = \sin^{-1}\left(\frac{W}{V}\sin\beta\right)$$

Considering the torque of the blade and the angular velocity resulting from the revolution of the turbine, the power of the turbine is:

$$Power_{rotor}\left[Watt\right]=T_{rotor}\left[N/m\right].\omega_{rotor}\left[rad/s\right] \tag{12}$$

Therefore, to design the turbine, the first step was to calculate the torque and power of the turbine based on the flow direction and the geometric characteristics of the turbine, which were investigated in this research for different flow speed states. From the perspective of the feasibility of optimal wind flow absorption and the improvement of aerodynamic indicators, the study of the interaction between the structure and the one-dimensional fluid, or the aerodynamic analysis of the flow around the blade, was mentioned. In this context, the turbulent flow around the blade was introduced in a stable and incompressible form using the k-ω shear stress transport turbulence model. Several important parameters, such as the pressure coefficient (CP) and the power factor (TSR), were explored to explain the flow behavior more precisely[33]. As mentioned, the power absorbed by the wind turbine was directly related to the air density, the surface area swept by the blades (in other words, the radius of the turbine blade), and the cube of the wind speed. However, the maximum turbine power absorbed was always less than this value. Additionally, the power factor of the rotor was assessed as described below.

$$C_p=\frac{P_{rotor}\left[W\right]}{0.5\rho A_{out}V_{\infty}^{3}\left[W\right]} \tag{13}$$

3. RESULTS & DISCUSSION

3.1. Analysis of the fluid-structure interaction of the turbine blade

In this section, the interaction between the structure and the fluid was investigated using Computational Fluid Dynamics (CFD). Then, based on the output from the previous section, the changes in dynamic parameters were studied, considering different types of turbine blades. To obtain the power coefficients for different tip speed ratios, simulations were Performed with a fixed value of wind speed and rotor rotation speeds ranging from 50 rpm to 500 rpm. The simulation conditions were Summarized in Table 2. From the simulation results, a graph of the power factor was obtained according to the tip speed ratio.

Table 2: Power factor simulation conditions for coding purposes

Parameter	Value	Unit
V_{∞}	12-20	m/s
ω	50-500	rpm

The Figure 6, shows the change in power factor (TSR) via wind speed (m/s).

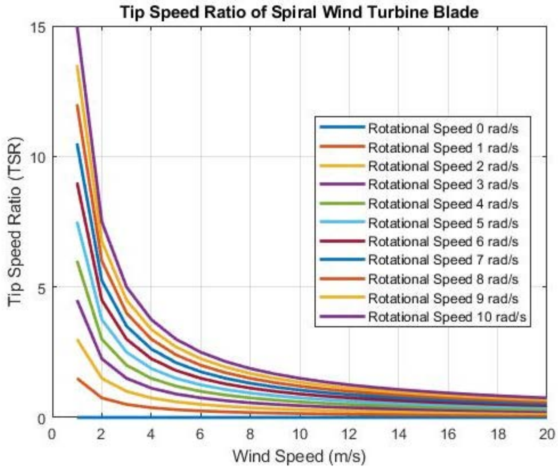

Figure 6: variation of TSR versus rotational speed.

The following chart illustrates the changes in the Power Factor Relative to the Tip Speed Ratio (TSR) and Wind Speed for Various Wind Speeds of 3.5, 4, and 4.5 m/s. It was observed, based on the Figure, that the Power Factor was less than 0.35, which was achieved at a Tip Speed Ratio of 10. This Ratio is actually the optimal Tip Speed Ratio estimated for the Turbine configuration, as Shown in Figure 7.

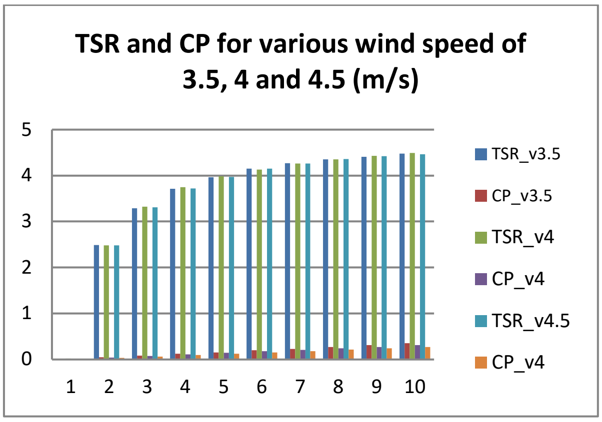

Figure 7: Variations of power factor with respect to TSR at air flow speed of 3.5, 4 and 4.5 m/s

According to the results obtained for different types of turbines, it is possible to calculate the results of power, TSR and specific parameters of each turbine and predict the performance of each one.

3.2. fluid-structure interaction

In this section, the analysis was conducted using the computational fluid dynamics (CFD) method and the ANSYS CFX multipurpose analyzer. The codes and equations were based on the Reynolds and Navier-Stokes equations. The dimensions of the channel were estimated to be approximately 0.8 × 8.0 × 1.5 meters. For this purpose, the blade and the flow passage channel were first modeled in the software. Then, the meshing of the fixed and rotating spaces was simulated for the channel and the turbine blade, respectively, using the Multiple Frames of Reference (MFR) method (Figure 8).

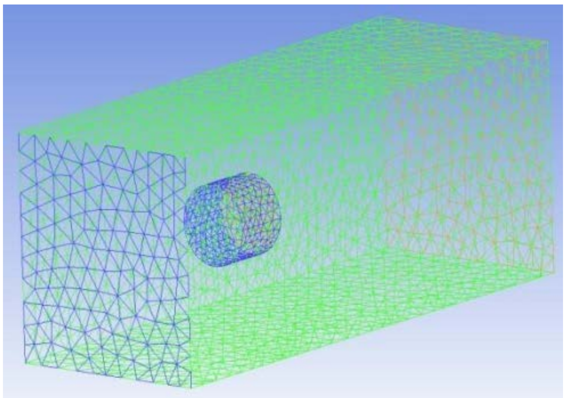

Figure 8 Simulation of fixed and rotating space

In this research, the performance analysis of the 0.5 kW spiral turbine was considered in terms of the number of elements, with approximately 370,584 elements for the fixed space and 470,584 elements for the rotating space. The ANSYS WORKBENCH software, CFX, and Static Structure modules, along with the FSI (Fluid-Structure Interaction) analysis method, were used for the phenomenon simulation. The meshing of the parts in both environments was performed using the dimensions and shape of the parts with a Free mesh type and sizing tools. First, the turbine was simulated in the CFX environment according to the environmental conditions around the shaft axis with a specific rotational speed. By incorporating the pressure and flow velocity parameters on the turbine blades and loading the fluid simulation results into the static structural environment, the stresses and deformation of the turbine were evaluated.

Table 3 The number of fixed and rotating range elements

Domain Name	**Element Number**
Fixed Domain	370584
Rotating Domain	470684
Total Domain	841168

Additionally, three modes of inlet speed—3.5, 4, and 4.5 m/s—were used, along with angular speeds of 300, 400, and 500 rpm to simulate the turbine with specific boundary conditions. The boundary conditions around the turbine were set to zero Pascal at the top, bottom, and sides. Finally, the values of mass flow rate and momentum in the free space were applied to all three blades of the turbine, and the amount of airflow at the inlet and outlet of the turbine was calculated using the boundary conditions of the connections between the elements. As mentioned, the fluid interaction analysis was evaluated to improve the performance of the spiral turbine blades. Figure 9shows the pressure contour lines in front of and behind the blades at a Tip Speed Ratio (TSR) of 2.5. These images demonstrate that the pressure in front of the turbine blades (upstream side) is higher than behind the blades (downstream side).

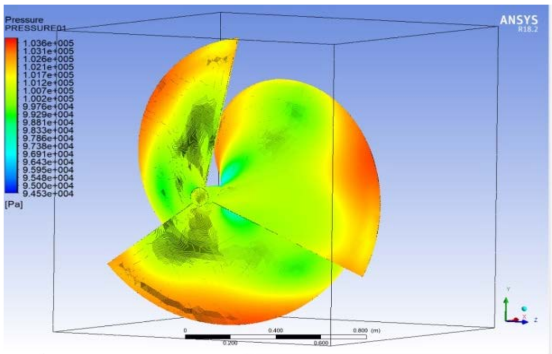

(a)

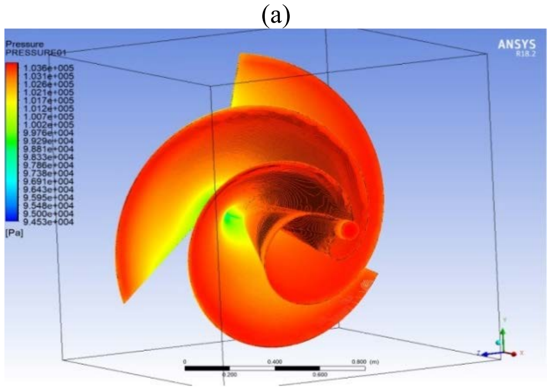

(b)

Figure 9: (a) and (b) show the minimum pressure behind the turbine blade and the maximum pressure in front of the turbine blade, respectively, with a rotational speed of 55 rad/s and an inlet velocity of 4.5 m/s.

During the laboratory simulation, the wind flow entered the turbine blades, creating a pressure difference between the front and back sides. The spiral design of the blades led to the generation of a force due to this pressure difference. The speed contour of the flow is depicted in Figure 10.

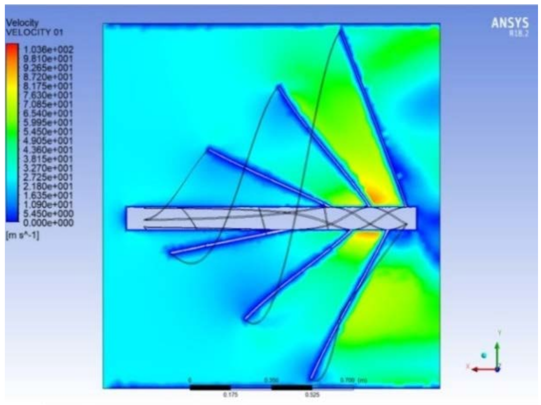

Figure 10 The speed contour around, center, and near the shaft, with a rotational speed of 55 rad/s and an inlet velocity of 4.5 m/s,

As can be seen, the flow velocity reached its lowest value in the center and near the shaft. As expected, the highest flow velocity occurred in the tip region, where the tip velocity was higher than in the central region. The wind flow at the tips of the blades created torque, causing the turbine blades to rotate in the opposite direction of the direct flow. Due to the helix effect, leading-edge velocities increased on the inner side of each blade. A lower velocity recirculation zone was also observed as the inlet airflow was blocked by the hub cone and rotor. This meant that there was a circular acceleration zone behind the rotor, resulting in low pressure near the wall of the rotating domain. For this reason, a low-speed zone formed behind the rotor hub. In the same Way, the pressure coefficient (CP) and the Tip Speed Ratio (TSR) were considered as two important factors in the study of turbine performance [13, 34, 35].

3.3. Investigating the deformation of printed PLA wind turbine

The intended assembly was a wind turbine with spiral blades made of PLA material, reinforced by steel rods. After various simulations, the thickness of the turbine blades was considered to be 4 mm. In this analysis, simulations were conducted for blades with thicknesses of 4 and 5 mm without steel bars. Due to the weight and behavior of the turbine blades, a thickness of 4 mm was chosen, and steel bars were used for each blade, connected by nuts. The simulation in this section was conducted for a rotational speed of 55 radians/s (500 to 525 rpm) and a flow inlet velocity of 3.5 m/s. The simulation was performed using ANSYS Workbench software with the Static Structure module. The connections in the software were of cylindrical type, fixed in Axial and Radial modes, and free in Tangential mode. The boundary condition and mesh refining are presented at Figure 11and Figure 12.

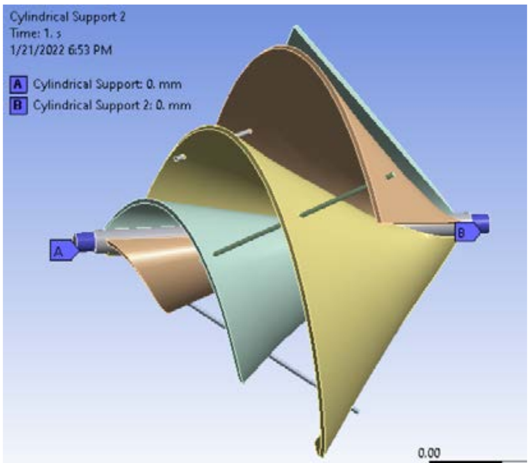

Figure 11: boundary condition

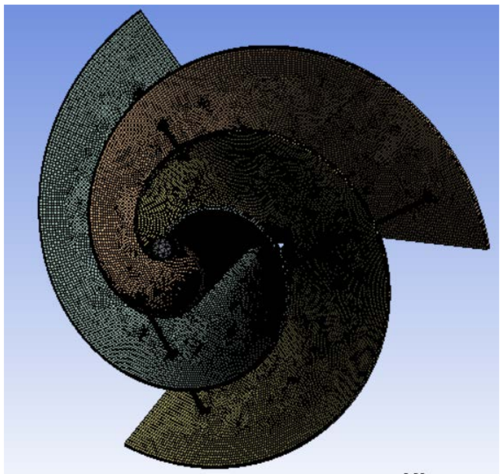

Figure 12: Blade meshing for interaction analysis

As seen, in, the boundary conditions including the

As seen in Figure 11, the boundary conditions, including the type of support and the direction of the rotational speed of the blade, were shown. In the ANSYS Workbench software, 16,246 elements were used for the finite element modeling of the turbine blade. The elements were of free mesh type, and their shape and size were modified using sizing and refining tools.

3.4. Analysis results of PLA turbine blade structure with 4 mm thick blade

In this section, the results of the analysis of the interaction between the fluid and the structure of the turbine with a 4 mm thick blade were reviewed and reported. The results of the static analysis, which arise from the interaction of the fluid with the structure, shown. Specifically, two parameters, the maximum stress in the blade and the maximum displacement of the blade due to fluid flow, were evaluated. The results of changing the blade length are reported as follows.

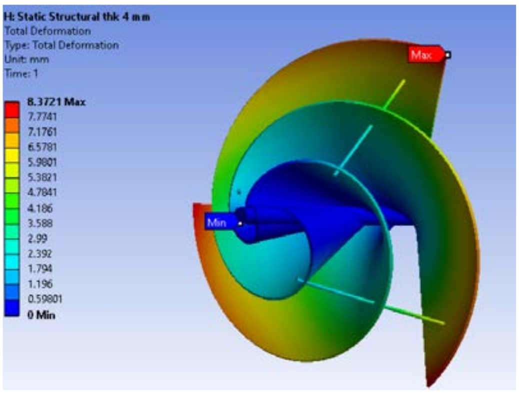

(a)

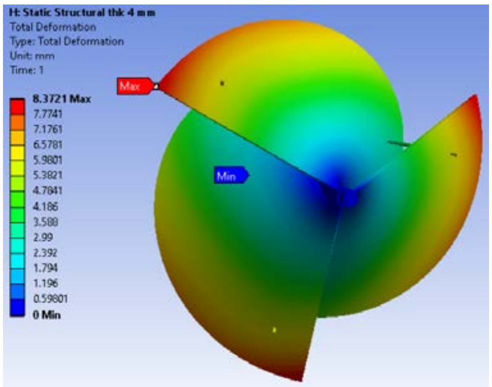

(b)

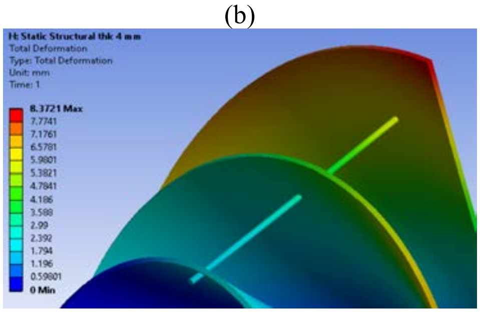

(c)

Figure 13: (a) to (c), different sections of the total deformation of the PLA turbine blade at a rotational speed of 55 radians/s and an inlet speed of 3.5 m/s are shown.

As shown, the maximum and minimum displacement of the tip of the blade (in the analysis results of the structure of the wind turbine blade made of PLA and 4 mm thick) was 8.3 mm, which was estimated to be 2.1% of the axial length of the blade (378 mm). Also, as seen in Figure 27, the maximum amount of stress in the connecting rods was estimated at 97.3 MPa, which was within the safe range in terms of design due to the steel material of the rods.

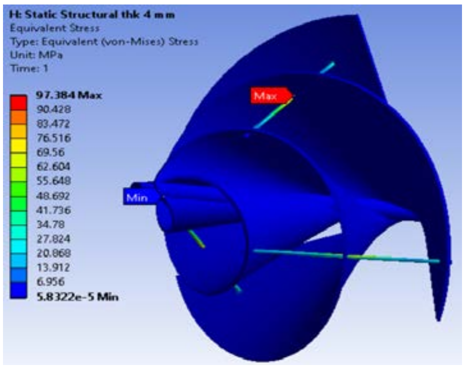

(a)

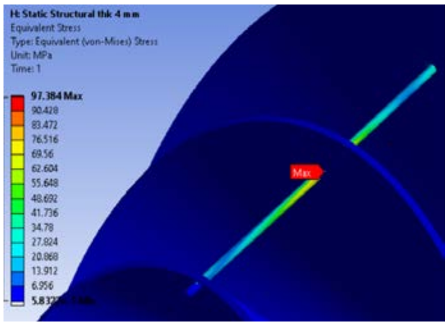

(b)

Figure 14: The highest stress on PLA rods at a rotational speed of 55 radians/s and an input speed of 3.5 m/s

As can be seen, the maximum stress occurs at the point of connection between the blade and the rod, which should increase the strength of the rods in higher speed flows.

3.5. Investigating the deformation of the steel plate wind turbine assembly

In the first stage, the results of the static structure were performed at a speed of 4.5 m/s and different rotational speeds of 300, 400, and 500 rpm. In the second stage, the results were checked at 500 rpm with different speeds of 3.5, 4, and 4.5 m/s. The steel plate with a thickness of 1 mm was considered according to the thicknesses available in the market. In this section, three types of materials were considered, which are shown in the table below.

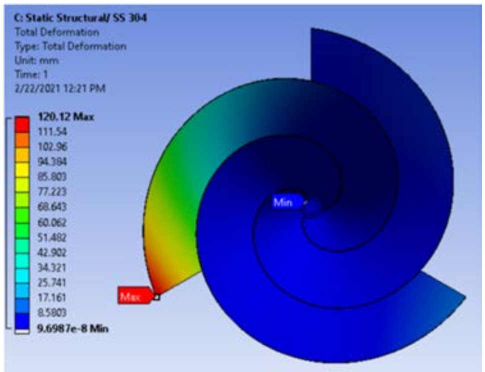

(a)

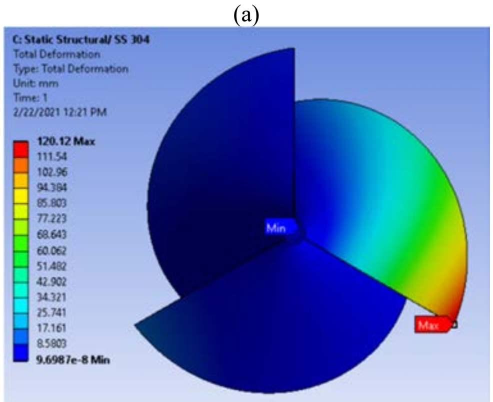

(b)

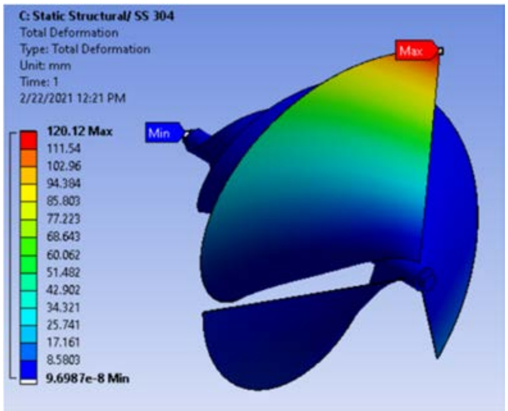

(c)

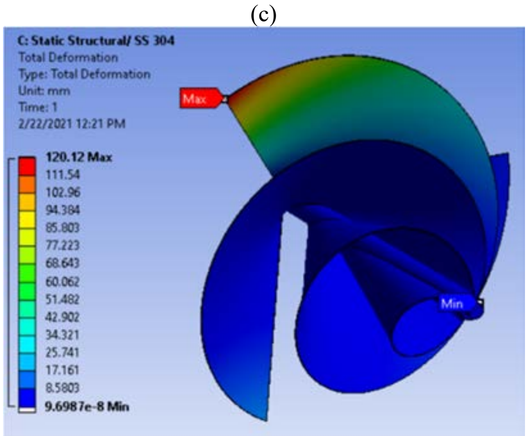

(d)

Figure 15: (a) to (d), Deformation of stainless steel (SS 304) at a rotational speed of 500 (RPM) and a speed of 3.5 m/s

As you can see, the maximum displacement of the blade tip (critical point) will be 120 mm (12 cm). A similar analysis was done to obtain the amount of stress applied to the blade.
Wind speeds and rotational speeds are varied in wind turbine experiments to analyze their effects on blade deformation, performance, and safety. Understanding these relationships is crucial for optimizing wind turbine design and ensuring safe operation. Wind speed in natural environments is variable, and turbines must be able to perform well under low wind conditions (wind shear) as well as high wind conditions (storm winds). The variation in rotational speed is also based on turbine control for optimal power generation. For example, at low wind speeds, turbines should be capable of generating energy at minimum rotational speeds. In contrast, during strong winds, the system must operate without damage and maintain stable performance [36] . Changes in wind speed and rotation lead to changes in aerodynamic forces and stresses applied to the blades. Analyzing the behavior of the blades at different speeds helps identify critical conditions and prevent material failure or fatigue. For instance, stresses from cyclic loading at varying speeds can reduce the lifespan of materials [37]. Different wind and rotational speeds are crucial for optimizing blade design and selecting effective materials. Studying these variables allows for improvements in blade performance and reductions in manufacturing and maintenance costs. For example, lightweight, high-strength materials are preferred for high-speed and heavy load conditions [38].Turbines need to operate stably across various wind speeds. Studying dynamic behavior under different conditions helps design control systems that minimize fluctuations and improve energy efficiency[39]. At high wind speeds, the wind's excitation frequency may approach the blade's natural frequency, leading to resonance. Considering various wind speeds helps prevent such risks [40].

The results of von Mises stress of stainless steel (SS304) are shown as follows for 500 rpm and speed of 3.5 m/s.

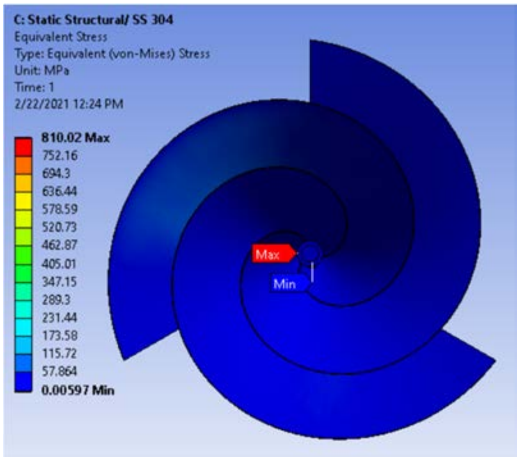

(a)

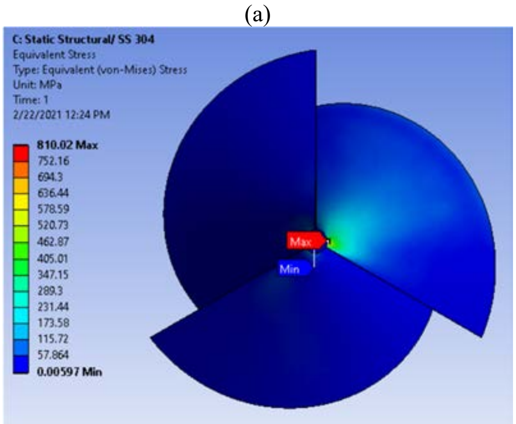

(b)

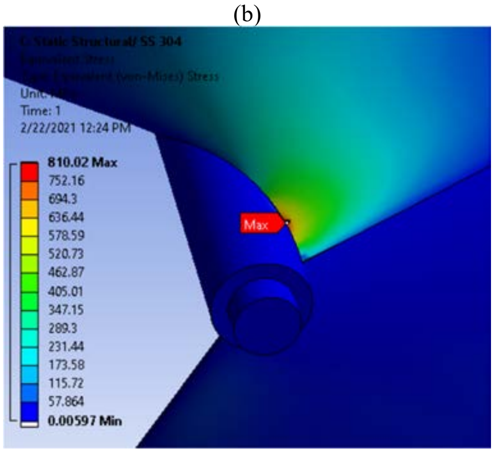

(c)

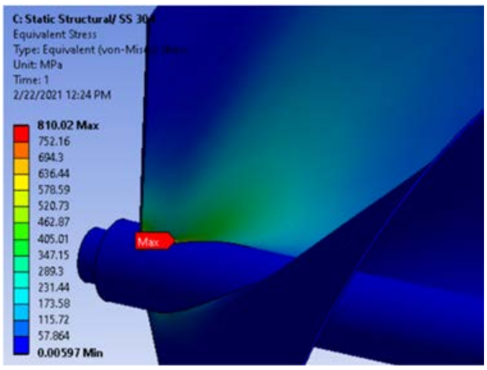

(d)

Figure 16: Von Mises stress of stainless steel (SS304) at 500 rpm and speed of 3.5 m/s.

As can be seen, the maximum amount of stress for stainless steel (SS 304) at 500 rpm and a speed of 3.5 m/s occurs at the root of the blade, the maximum value of which is 810 MPa. In other cases, the blade is not in critical condition. Therefore, it is better to make the blade stronger at the root (connection to the shaft). Also, the deformation of the stainless-steel blade (SS 304) coated with composite (glass/epoxy) will be as follows.

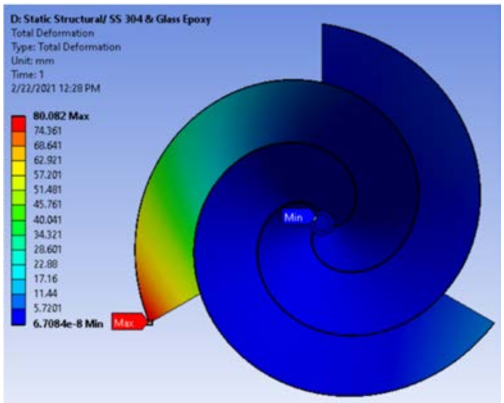

(a)

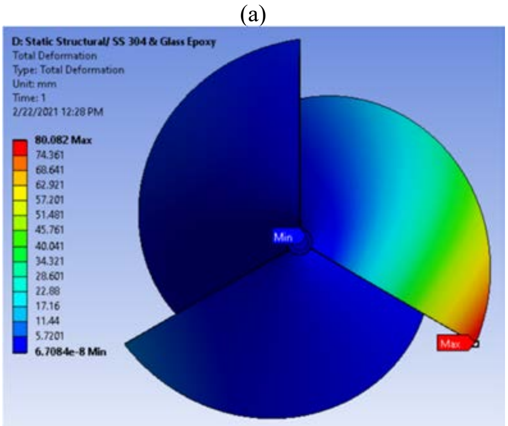

(b)

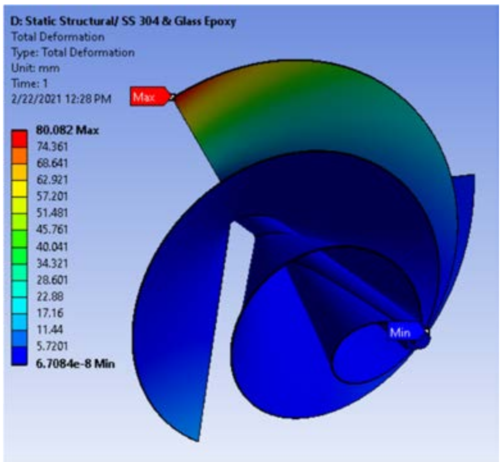

(c)

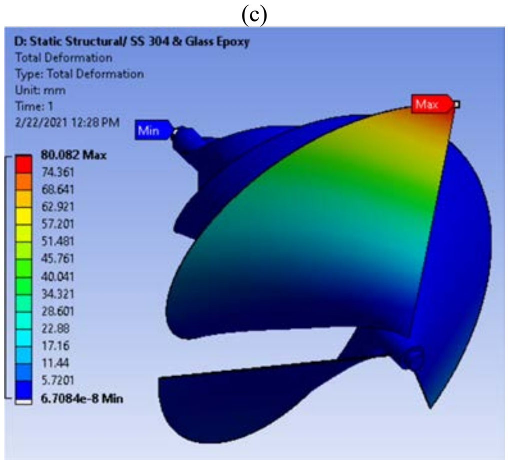

(d)

Figure 17 Deformation of stainless steel (SS 304) coated with epoxy glass composite at 500 RPM and speed of 3.5 m/s

The figure shows the maximum displacement of the tip of the blade (critical point) will be 80 mm (8 cm), which, according to the design, should be reinforced with a composite layer. A similar analysis was performed to obtain the amount of stress applied to the blade coated with glass/epoxy composite, the results of which are reported below.

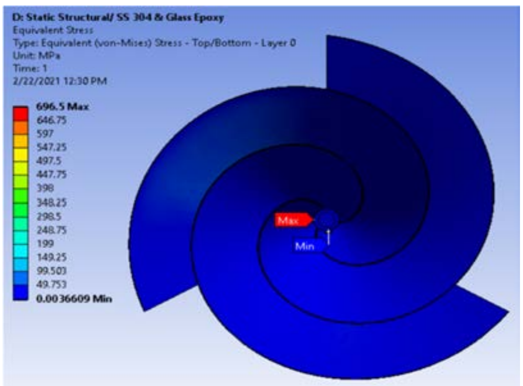

(a)

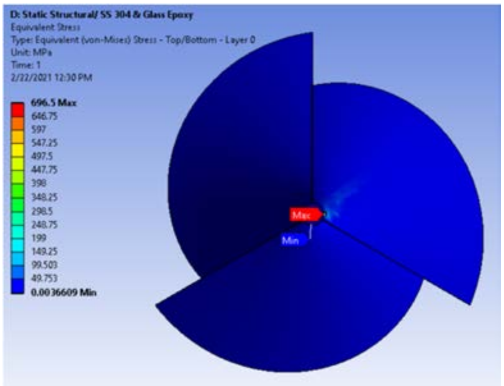

(b)

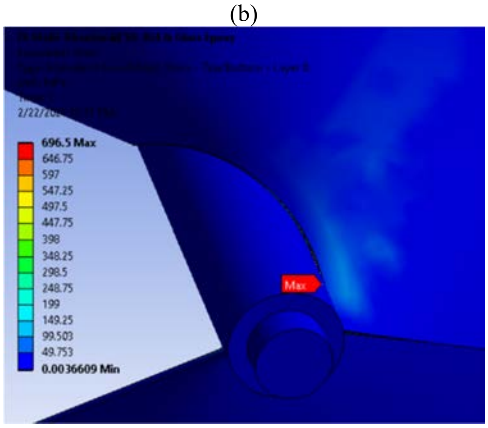

(c)

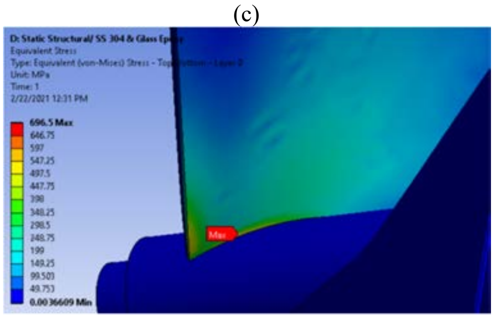

(d)

Figure 18: (a) to (d), Von Mises stress of stainless steel (SS304) coated with glass/epoxy composite at 500 rpm and speed of 3.5 m/s.

According to the single-layer composite coating (according to Table 4 t0 6), the critical stress in the blade has decreased compared to the all-metal blade, which indicates the higher strength of the blade with composite coating. In this case, the maximum amount of stress applied to the blade at the root is 696.5 MPa. Therefore, it is possible to obtain the results of blade stress and deformation according to the linear and rotational speeds of the wind. The relevant pseudo-static analysis is reported as follows in the below tables.

Table 4: Analysis results of 304 steel blade at different flow rates and different rotational speeds of the blade

Velocity (m/s)	**RPM**	**Stress (MPa)**		**Deformation (mm)**	
		Max	**Min**	**Max**	**Min**
4.5	300	798.57	0.006	124.22	0.0000000338
4.5	400	811.04	0.007	119.56	0.0000000118
4.5	500	942.39	0.004	140.09	0.0000001
4	500	851.54	0.004	126.29	0.000000049
3.5	500	810.02	0.005	120.12	0.000000096

Table 5: Analysis results of coated 304 steel blade at different flow speeds and different rotational speeds of the blade

		SS 304 & Glass Epoxy (Type 1)		SS 304 & Glass Epoxy (Type 2)		SS 304 & Glass Epoxy (Type 3)	
Velocity (m/s)	RPM	Stress (MPa)		Stress (MPa)		Stress (MPa)	
		Max	Min	Max	Min	Max	Min
4.5	300	685.99	0.003	691.23	0.004	694.19	0.004
4.5	400	696.98	0.004	701.9	0.004	704.93	0.004
4.5	500	810.82	0.006	816.65	0.003	820.16	0.003
4	500	732.49	0.002	737.48	0.004	740.67	0.004
3.5	500	696.5	0.003	701.23	0.003	704.27	0.003

Table 6: Analysis results of coated 304 steel blade at different flow speeds and different rotational speeds of the blade

		SS 304 & Glass Epoxy (Type 1)		SS 304 & Glass Epoxy (Type 2)		SS 304 & Glass Epoxy (Type 3)	
Velocity(m/s)	RPM	Deformation (mm)		Deformation (mm)		Deformation (mm)	
		Max	Min	Max	Min	Max	Min
4.5	300	82.47	0.000000027	81.29	0.00000001	82.88	0.000000034
4.5	400	79.38	0.00000003	78.23	0.0000027	79.73	0.0000016
4.5	500	92.98	0.0000057	91.62	0.0000041	93.39	0.00000017
4	500	84.19	0.000000011	82.6	0.000000058	84.2	000000026
3.5	500	80.08	0.0000067	78.58	0.00000017	80.1	0.000000084

The choice between polymer composite coatings and metal matrix composite (MMC) coatings for metallic wind turbine blades involves considering adhesion strength, crack propagation, and overall performance. While polymer composites like epoxy/glass or carbon are commonly used, MMCs offer unique advantages, though their adoption depends on specific design requirements and trade-offs.

4.CONCLUSION

The current study examined the effect of coatings on the dynamic behavior of rotating composite turbine blades. It specifically analyzed carbon/epoxy and glass/epoxy coatings applied to metal blades, taking into account the interaction between the structure and fluid. The results revealed that the use of composite coatings on blades resulted in a significant enhancement in dynamic performance, strength, and aerodynamic efficiency compared to traditional metal blades. It was observed that the use of composite coatings on blades increased the strength of the blade and thus increased the Natural Frequencies of the blade.

5. REFERENCES

[1] R. Howell, N. Qin, J. Edwards, and N. Durrani, "Wind tunnel and numerical study of a small vertical axis wind turbine," *Renewable energy,* vol. 35, no. 2, pp. 412-422, 2010. https://doi.org/10.1016/j.renene.2009.07.025

[2] M. Arifujjaman, M. T. Iqbal, and J. E. Quaicoe, "Energy capture by a small wind-energy conversion system," *Applied Energy,* vol. 85, no. 1, pp. 41-51, 2008. https://doi.org/10.1016/j.apenergy.2007.06.002

[3] Z. Simic, J. G. Havelka, and M. B. Vrhovcak, "Small wind turbines–A unique segment of the wind power market," *Renewable Energy,* vol. 50, pp. 1027-1036, 2013. https://doi.org/10.1016/j.renene.2012.08.038

[4] M. Bortolini, M. Gamberi, A. Graziani, R. Manzini, and F. Pilati, "Performance and viability analysis of small wind turbines in the European Union," *Renewable Energy,* vol. 62, pp. 629-639, 02/01 2014. https://doi.org/10.1016/j.renene.2013.08.004

[5] C.-M. Sung and M.-C. Han, "Design and performance evaluation of hinge type pitch control system in small-size wind turbine," *International Journal of Precision Engineering and Manufacturing-Green Technology,* vol. 3, no. 4, pp. 335-341, 2016.https://doi.org/10.1007/s40684-016-0042-2

[6] J.-H. Kim, H.-D. Yang, K.-J. Lee, S.-D. Song, S.-H. Park, and J.-H. Shin, "An Experiment on power properties in a small-Scaled Wind Turbine Generator," *Journal of power and energy engineering,* vol. 1, no. 7, pp. 6-13, 2013. https://doi.org/10.4236/jpee.2013.17002

[7] E. A. Arens and P. B. Williams, "The effect of wind on energy consumption in buildings," *Energy and Buildings,* vol. 1, no. 1, pp. 77-84, 1977.https://doi.org/10.1016/0378-7788(77)90014-7

[8] F. Balduzzi, A. Bianchini, E. A. Carnevale, L. Ferrari, and S. Magnani, "Feasibility analysis of a Darrieus vertical-axis wind turbine installation in the rooftop of a building," *Applied Energy,* vol. 97, pp. 921-929, 2012. https://doi.org/10.1016/j.apenergy.2011.12.008

[9] H. Hirahara, M. Z. Hossain, M. Kawahashi, and Y. Nonomura, "Testing basic performance of a very small wind turbine designed for multi-purposes," *Renewable energy,* vol. 30, no. 8, pp. 1279-1297, 2005. https://doi.org/10.1016/j.renene.2004.10.009

[10] F. Scheurich and R. E. Brown, "Modelling the aerodynamics of vertical-axis wind turbines in unsteady wind conditions," *Wind Energy,* vol. 16, no. 1, pp. 91-107, 2013. https://doi.org/10.1002/we.532

[11] S.-M. Yang, H.-S. Ji, D.-S. Shim, J.-H. Baek, and S.-H. Park, "Conical roll-twist-bending process for fabrication of metallic archimedes spiral blade used in small wind power generator," *International Journal of Precision Engineering and Manufacturing-Green Technology,* vol. 4, no. 4, pp. 431-439, 2017. https://doi.org/10.1007/s40684-017-0048-4

[12] W. Timmer and S. Toet, "Verslag van de metingen aan de archimedes in de lage-snelheids windtunnel van dnw," *TU Delft,* 2009.https://doi.org/10.18174/533390

[13] K. C. Kim, H. S. Ji, Y. K. Kim, Q. Lu, J. H. Baek, and R. Mieremet, "Experimental and numerical study of the aerodynamic characteristics of an archimedes spiral wind turbine blade," *Energies,* vol. 7, no. 12, pp. 7893-7914, 2014. https://doi.org/10.3390/en7127893

[14] T. Matsushima, S. Takagi, and S. Muroyama, "Characteristics of a highly efficient propeller type small wind turbine with a diffuser," *Renewable Energy,* vol. 31, no. 9, pp. 1343-1354, 2006.https://doi.org/10.1016/j.renene.2005.07.008

[15] W. D. Lubitz, "Impact of ambient turbulence on performance of a small wind turbine," *Renewable Energy,* vol. 61, pp. 69-73, 2014.https://doi.org/10.1016/j.renene.2012.08.015

[16] J. O. Dabiri, "Potential order-of-magnitude enhancement of wind farm power density via counter-rotating vertical-axis wind turbine arrays," *Journal of renewable and sustainable energy,* vol. 3, no. 4, p. 043104, 2011. https://doi.org/10.1063/1.3608170

[17] H. S. Ji, L. Qiang, J. H. Beak, R. Mieremet, and K. C. Kim, "Effect of the wind direction on the near wake structures of an Archimedes spiral wind turbine blade," *Journal of Visualization,* vol. 19, no. 4, pp. 653-665, 2016. https://doi.org/10.1007/s12650-016-0356-8

[18] S. Chaudhary, S. Jaiswal, R. Nanda, S. Patel, and P. Kumar, "Comparison of torque characteristics of Archimedes wind turbine evaluated by analytical and experimental studyl," *International Journal of Mechanical and Production Engineering,* vol. 4, no. 8, pp. 75-78, 2016.

[19] A. Safdari and K. C. Kim, "Aerodynamic and structural evaluation of horizontal archimedes spiral wind turbine," *Journal of Clean Energy Technologies,* vol. 3, no. 1, pp. 34-38, 2015.https://doi.org/10.7763/jocet.2015.v3.164

[20] T. Saroinsong, R. Soenoko, S. Wahyudi, and M. N. Sasongko, "Fluid flow phenomenon in a three-bladed power-generating Archimedes screw turbine," *Journal of Engineering Science and Technology Review,* vol. 9, no. 2, pp. 72-79, 2016. https://doi.org/10.25103/jestr.092.12

[21] T. Burton, D. Sharpe, N. Jenkins, and E. Bossanyi, *Wind energy handbook*. Wiley Online Library, 2001. https://doi.org/10.1002/0470846062

[22] G. Abad, A. Plaza, and G. J. S. C. Kerejeta, "Performance Evaluation of Small Wind Turbines Under Variable Winds of Cities: Case Study Applied to an Ayanz Wind Turbine with Screw Blades," vol. 7, no. 6, pp. 3241-3288, 2024. https://doi.org/10.3390/smartcities7060126

[23] J. Prananda, E. S. Koenhardono, N. F. J. I. J. o. M. E. I. Farhan, and Research, "Performance Analysis of Screw Turbine Design with additional flaps modification using computational fluid dynamics method," vol. 6, no. 4, pp. 246-254, 2021. https://doi.org/10.12962/j25481479.v6i4.10623

[24] A. T. Ubando *et al.*, "Sustainable Manufacturability of Archimedes Screw Turbines: A Critical Review," vol. 6, no. 6, p. 161, 2022.https://doi.org/10.3390/jmmp6060161

[25] K. C. Kim, H. S. Ji, Y. K. Kim, Q. Lu, J. H. Baek, and R. Mieremet, "Article Experimental and Numerical Study of the Aerodynamic Characteristics of an Archimedes Spiral Wind Turbine Blade," 2014.https://doi.org/10.3390/en7127893

[26] R. Kot, M. Rolak, and M. Malinowski, "Comparison of maximum peak power tracking algorithms for a small wind turbine," *Mathematics and Computers in Simulation,* vol. 91, pp. 29-40, 2013.https://doi.org/10.1016/j.matcom.2013.03.010

[27] A. M. Labib, A. F. A. Gawad, M. M. J. J. o. A. R. i. F. M. Nasseif, and T. Sciences, "Effect of blade angle on aerodynamic performance of Archimedes spiral wind turbine," vol. 78, no. 1, pp. 122-136, 2021. https://doi.org/10.37934/arfmts.78.1.122136

[28] H. Ji, K. C. Kim, J. H. Baek, and R. J. J. o. P. S. Ruijtenbeek, "The aerodynamic method of the Archimedes Windturbine," 2014.https://doi.org/10.3390/en7127893

[29] K. C. Kim, H. S. Ji, Y. K. Kim, Q. Lu, J. H. Baek, and R. J. E. Mieremet, "Experimental and numerical study of the aerodynamic characteristics of an archimedes spiral wind turbine blade," vol. 7, no. 12, pp. 7893-7914, 2014. https://doi.org/10.3390/en7127893
[30] S. Sapkota, A. Bhattarai, H. P. Bashyal, and U. Nepal, "Design, CFD analysis and modelling of archimedean-spiral type wind turbine," in *Proc. IOE Grad. Conf*, 2019, vol. 6, pp. 563-571.
[31] A. Safdari and K. C. J. J. o. C. E. T. Kim, "Aerodynamic and structural evaluation of horizontal archimedes spiral wind turbine," vol. 3, no. 1, pp. 34-38, 2015. https://doi.org/10.7763/jocet.2015.v3.164
[32] D. Adinarayana, "Performance Study of Archimedes Spiral Wind Turbine using Numerical and Experimental Analysis," *International Journal for Research in Applied Science and Engineering Technology,* vol. 7, pp. 57-67, 08/31 2019. https://doi.org/10.22214/ijraset.2019.8008
[33] S. Ebrahimi and M. A. Ghassemi, "Numerical aerodynamics analysis of the of the Archimedes screw wind turbine," *Int. J Multidisciplinary Sci & Eng,* pp. 12-15, 2018. https://doi.org/10.3390/en7127893
[34] F. Porté-Agel, Y.-T. Wu, H. Lu, and R. J. Conzemius, "Large-eddy simulation of atmospheric boundary layer flow through wind turbines and wind farms," *Journal of Wind Engineering and Industrial Aerodynamics,* vol. 99, no. 4, pp. 154-168, 2011. https://doi.org/10.1016/j.jweia.2011.01.011
[35] N. J. Choi, S. H. Nam, J. H. Jeong, K. C. J. J. o. W. E. Kim, and I. Aerodynamics, "Numerical study on the horizontal axis turbines arrangement in a wind farm: Effect of separation distance on the turbine aerodynamic power output," vol. 117, pp. 11-17, 2013.https://doi.org/10.1016/j.jweia.2013.04.005
[36] T. Burton, N. Jenkins, D. Sharpe, and E. Bossanyi, *Wind energy handbook*. John Wiley & Sons, 2011. https://doi.org/10.1002/0470846062
[37] H. J. Sutherland, "On the fatigue analysis of wind turbines," 1999.https://doi.org/10.2172/9460
[38] J. F. Manwell, J. G. McGowan, and A. L. Rogers, *Wind energy explained: theory, design and application*. John Wiley & Sons, 2010.https://doi.org/10.1002/9781119994367
[39] M. Hansen, *Aerodynamics of wind turbines*. Routledge, 2015. https://doi.org/10.4324/9781315769981
[40] P. S. Veers *et al.*, "Trends in the design, manufacture and evaluation of wind turbine blades," *Wind Energy: An International Journal for Progress and Applications in Wind Power Conversion Technology,* vol. 6, no. 3, pp. 245-259, 2003.https://doi.org/10.1002/we.90

Appendix A:

Designing procedure

The spiral turbine mainly consists of three spiral blades, a generator, a magnetic brake, a frame, and a Yawing jig, as shown in
Figure 1. Among these components, the most important is the blade, which has a completely different shape than the general case, and the blade system is such that three helical blades are arranged at equal distances along a rotating shaft. However, due to its peculiar and complex shape, it is challenging to precisely manufacture the blade using conventional manufacturing processes. The outline is an Archimedean spiral curve that changes continuously, so the center point of each curve changes according to the outline. The designed geometry of a helical blade and the overall shape of the Archimedean conical blades surrounded by spline curves are shown in Figure 19.

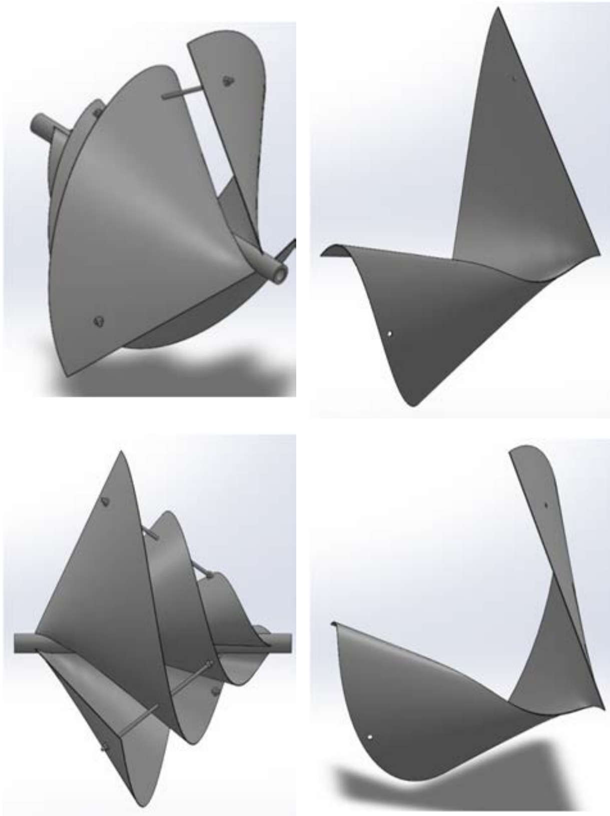

Figure 19 Blade sample designed by plate forming process

As shown in Figure 19, first, the wide surface of the plate is designed, and then, using the bending module, the plate is shaped into an Archimedean screw. The unfolded view of the plate used for the blade is shown in Figure 20 as well.

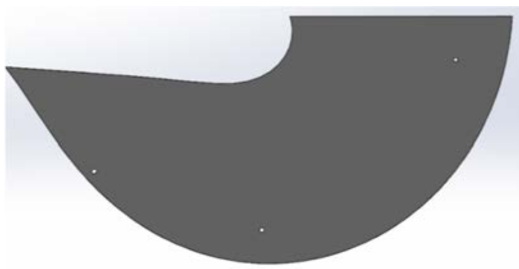

Figure 20 Exploded view of the plate used for the blade

One of the methods of plate bending and blade creation is a new roller-forming process called Roll-twist-bending (RTB), which is divided into two types. Since it is not easy to make a shaping stage without changing the central points, it is necessary to divide the blade into several parts for multi-stage shaping. It is obvious that these steps are only to design and manufacture the metal blade and it is not used for the composite and polymer ones (which are used in this research in addition to the metal blade). As shown in Figure 21, the ideal is to create the number (N) of dividing sections to achieve accurate curvature, which in this research, these sections are six.

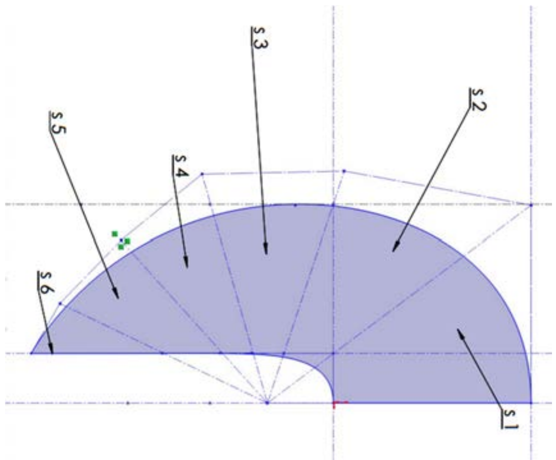

Figure 21 Six different parts of the blade

In the case that the plate is divided into several parts, Fibonacci relations are used to estimate the value of each part. In other words, the Fibonacci relationship is a measure to accurately determine the geometry of each section. In this method, considering that after the sixth section, the Fibonacci ratio practically remains constant, the number of desired sections for forming the plate is six. The relationships related to the Fibonacci theory are presented below.

$$F(n)=\frac{\varphi^{n}-(1-\varphi)^{n}}{\sqrt{5}}=\frac{\varphi^{n}-(-\varphi)^{-n}}{\sqrt{5}} \quad (14)$$

(□) is the golden number which is approximately equal to 1.6. As an example, the ratio of the second term to the first is calculated according to the above relation and by placing them as follows.

$$F(1)=\left(\frac{\left(\frac{1+\sqrt{5}}{2}\right)^{1}-\left(\frac{1-\sqrt{5}}{2}\right)^{1}}{\sqrt{5}}\right)=\frac{\frac{1+\sqrt{5}}{2}-\frac{1-\sqrt{5}}{2}}{\sqrt{5}}=\frac{\frac{\sqrt{5}+\sqrt{5}}{2}}{\sqrt{5}}=\frac{\frac{2\sqrt{5}}{2}}{\sqrt{5}}=1 \quad (15)$$

To achieve a continuously varying curvature, the blade was divided into six sections based on geometric analysis. Considering more or fewer than six sections would introduce complications in the rolling process, which will be discussed in the following. If the number of sections exceeds six, issues arise in creating curvature with the bending roller, such as an increase in the height (H) required to achieve the appropriate angle for sheet rotation relative to the x-axis. Naturally, as the number of sections increases, the angle between each section decreases, and consequently, the length (L) and the corresponding radius (R) in subsequent sections increase. According to the Fibonacci criterion, the obtained values of R depend on the initial L, which is selected based on the blade's overall dimensions and conditions. This necessitates a greater increase in H to achieve the required angle of approximately three degrees. If H is not increased, the angle φ must be adjusted, which in turn complicates the positioning of the bending roller alongside the conical roller and increases the number of adjustments needed for each section in the rolling mechanism .Although it is theoretically possible to achieve the desired curvature with more sections, around nine, it would require additional adjustments in the bending rollers, making the forming process more complex. Conversely, if fewer than six sections are considered, the curvature radius (R) may increase up to 45 degrees, causing the bending roller adjusted according to the angle of each section (θ) to move excessively away from the conical roller. This, in turn, complicates the rolling process as additional adjustments would be needed to ensure the sheet remains properly aligned on the bending roller and avoids deviations or excessive bending. Therefore, based on the above explanations, using six sections is optimal for achieving better performance and facilitating easier adjustment of the blade forming mechanism. In this design approach, only the initial value of L is required, which can be selected arbitrarily or based on the desired blade length. Other computational parameters will be determined automatically according to Fibonacci calculations. In other words, the Fibonacci relationships serve as a precise criterion for determining the geometry of each section. In this method, considering that the Fibonacci ratio remains constant after the sixth section, the optimal number of sections for shaping the sheet is determined to be six. The following presents the equations related to Fibonacci theory. According to the provided explanations, the design has been carried out based on the expansion of Fibonacci calculations and the golden ratio applied to lines and edges, and it has also been utilized in the manufacturing process.

The above calculations indicate that the appropriate amount of dividing the segments to create the curve is six segments. Considering more than this number of construction steps faces difficulty. Also, making allowance for more parts will not change much in the desired curvature. Figure 22 shows how to draw and segment the blade, which is drawn based on the extension of Fibonacci calculations and the golden ratio to lines and sides. According to the geometry of the Fibonacci spiral, the ratio of the large side to the small side of the rectangle in which the blade is drawn is 1.6. Using the method, the initial value L (only requirement), which can be selected based on the desired length for construction purposes. In the accompanying figure, s represents the area allocated to each section. Generally, the overview of the plate and rollers is as follows, where various parameters such as L, θ, ϕ, H, and others are detailed.

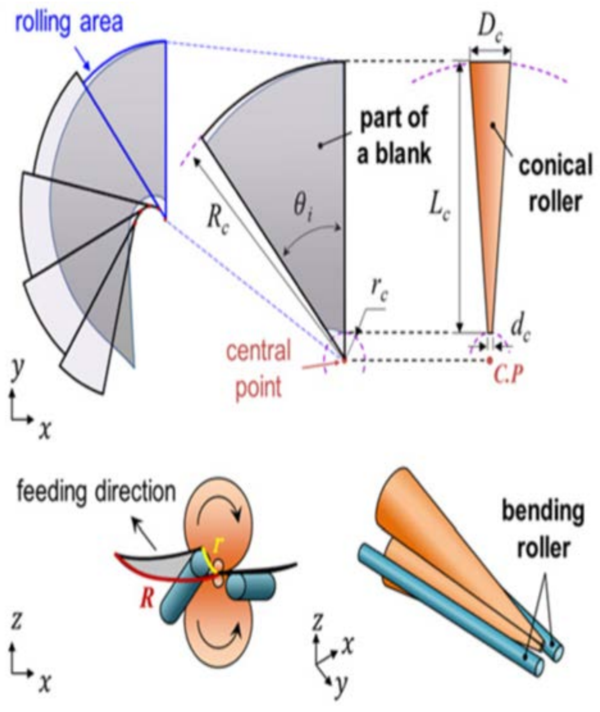

(a)

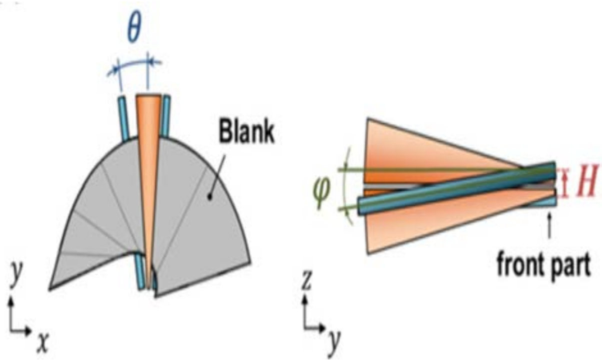

(b)

Figure 22 (a) Schematic diagram of roller and four-roller design: double tapered rollers and two bending rollers, (b) RTB process parameters. Z-axis rotation angle θ, motion H, and axis rotation angle φ.

In the above figure, the radius of curvature of the cross-section in the inner line (r_i line) with a certain distance (L) from the outline is called the inner curvature radius (r_i). Here, the amount of change in the radius of curvature (R) of each segment is called degrees (g_i).

$$g_i = \frac{R_i - r_i}{L} \tag{16}$$

The degree means the difference between two values R_i and r_i according to the distance (L), which shows the linear relationships, also, R_i and g_i of each part formed are summarized in Table 7.

Table 7: Radius of curvature and angle of each section, ΔR in each section, parameter L for each section

[1] The first part	[2] The second part	[3] The third part	[4] The fourth part	[5] The fifth part	[6] The sixth part	[7]
[8]	[9] 147.8	[10] 126.16	[11] 106.73	[12] 70.11	[13] 24.97	**[14] g_i (ΔR)**

On the other hand, the ratio of the external radius (R_c) to the internal radius (r_c) of the section and the ratio of the base diameter (D_c) and the upper diameter (d_c) of the conical roller are also the same. The dimensions of tapered rollers are simply calculated:

$$D_c = \frac{R_c \theta_i}{\pi} \times n$$
$$d_c = \frac{r_c \theta_i}{\pi} \times n \tag{17}$$

Where n is the number of rollers (which will be 1) if it is completely rotated in the roller area. I Table 8, the values of the base diameter (D_c) and the top diameter (d_c) of the conical roller in terms of the radius of curvature, the angle θ of each section, and the parameter g_i for each section are given.[1]

Table 8: The radius of curvature and the angle of each section θ, the parameter g_i for each section, and the dimensions of the conical rollers d_c, d_c (angles are in radians and sizes are in millimeters)

parameter	The First part	The Second part	The Third part	The Forth part	The Fifth part	The Sixth part	Average
g_i		0.93	0.81	0.73	0.69	0.58	
R_c	308	286.83	245.08	228.31	239.6	269.07	
r_c	77	69.03	56.95	59.56	80.34	135.76	
θ_i	0.64	0.6	0.59	0.46	0.4	0.45	

[1] On average, conical rollers with diameters of 45 and 14 mm are used in this process.

D_c	62.74	54.81	46.01	33.53	31	39	45
d_c	16	14	11	9	11	19	14

Cylindrical bending rollers are used on both sides of the tapered roller to create the curve by bending. Both ends of the bending rollers can be fixed or moved towards the twisting of the plate, and the angle between the bending rollers can be controlled. The controllable process variables are z-axis rotation angle (θ), movement amount (H), and x-axis rotation angle (φ) based on the front end of the bending roller as shown in Fig.10. A deformed shape of each part is determined by the process parameters, so it is necessary to optimize the parameters to deform a target shape in each part. Also, the bending center point must be reset at each step of the process. To conclude, in this study, an RTB process, consisting of upper and lower tapered rollers and a pair of lateral bending rollers, is proposed for the manufacture of the Archimedes spiral blade. To form continuous variable curvature, the blade was divided into six parts based on geometrical analysis. Considering more or less parts, some problems will arise in the rolling process, which will be discussed further. If the values of the sections are considered more than six, problems will arise in creating curvature with the bending roller, including the increase of H due to the creation of a suitable angle for the rotation of the plate relative to the x axis. It is obvious that with the increase in the number of sections, the angle between each section decreases and the value of length L and then R increases in the next sections (according to the Fibonacci criterion, the values of R obtained are dependent on the initial L value, which is based on the dimensions and general conditions of the blade is selected). This requires a further increase in H to create a suitable angle, which is around three degrees, and if H does not increase, the angle φ must be increased, in which case, placing the bending roller next to the conical roller and increasing the number of settings for each section in the All Equation must be in table and have a number and references in body same as Equation (1)

Numerical values of the dimensions of the turbine according to the design are shown as follows (

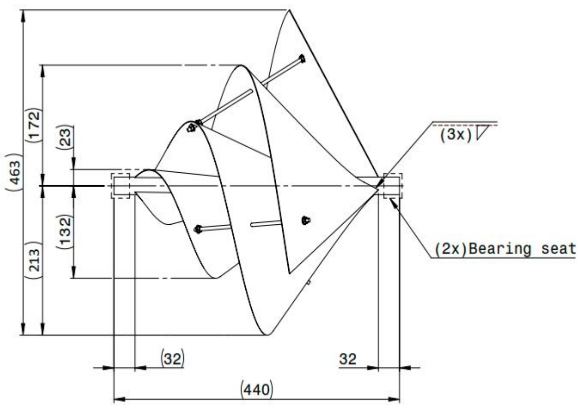

Figure 24: drawing the blade

mechanism, as a result of that, the rolling performance will cause problems. Of course, it should be kept in mind that it is possible to achieve the desired curvature with more sections, close to 9, but as explained, more adjustments should be made in the bending rollers, which makes the shaping more difficult. If less than six sections are considered, the radius of curvature angle R may increase up to 45 degrees, which makes the bending roller, which is adjusted to the angle of each section (□), far away from the conical roller, and this also causes problems in the rolling process. The reason is that more adjustment is needed so that the plate does not deviate or bend in the path of being placed on the bending roller. Therefore, according to the above explanation, it is better to consider the amount of six sections for better performance and easier adjustment of the blade-forming mechanism. By using water jet cutting, the plates were cut into blades based on the calculations and during the bending process. The thickness of the plate in the figures below is one mm and it is made of steel. Also, a general view of the machined rotor shaft attached to the blade is shown in Figure 23.

Figure 23 View of rotor shaftplate cut using laser cutting and metal blade

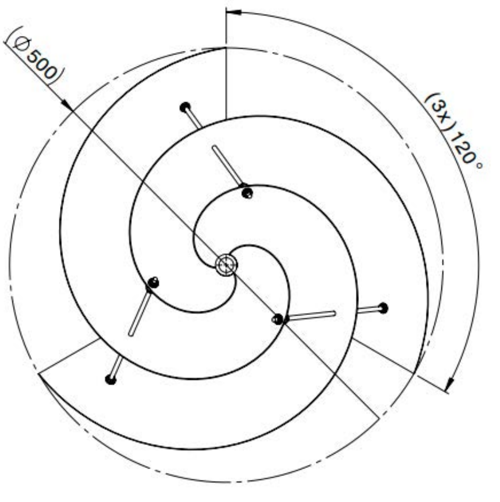

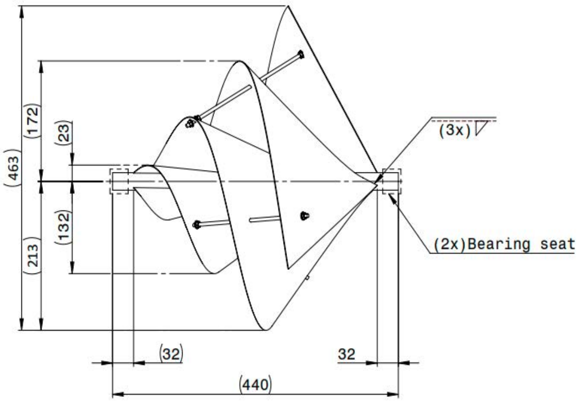

Figure 24 The dimensions of the 0.5 kW spiral turbine of the current research

Thus, the parameters of the shape and dimensions of the turbine in this research can be defined as follows (Table 9).

Table 9: Effective parameters in the turbine

Definition of the parameters	Parameter	Value	Unit
Inlet air density	ρ	1.225	kg/m^3
Inner radius	R_1	0.231	m
Outer radius	R_2	0.023	m
longitudinal distance	L1	0.138	m
longitudinal distance	L2	0.376	m
Rotational Velocity of the turbine	ω	52.35	rad/s
Blade end slope	β	0-120	degree
Inlet air velocity	V_∞	3.5/4/4.5	m/s

Definition of geometric parameters and relative speed components

The turbine shape parameters can be obtained through a geometric method, as shown in Fig.13, A_{out} can be expressed in terms of L1 and L2 (meaning the distance between the center of the rear side and the position x perpendicular to the tip of the blade is outer, and L2 designate the distance between the center position of the rear side and the position x, which is perpendicular to the tip of the inner blade).

$$\begin{aligned} A_{out} &= \frac{1}{2}R_2L_1 - \frac{1}{2}R_2L_1 + \frac{1}{2}\left(R_1 - R_2\right)\left(L_2 - L_1\right) \\ &= \frac{1}{2}\left(R_1 - R_2\right)L_2 \end{aligned} \tag{18}$$